JACS
JOURNAL OF THE AMERICAN CHEMICAL SOCIETY
pubs.acs.org/JACS
Article

Photocatalytic Molecular Oxygen Activation by Regulating Excitonic Effects in Covalent Organic Frameworks

Yunyang Qian, Dandan Li, Yulan Han, and Hai-Long Jiang*

Cite This: J. Am. Chem. Soc. 2020, 142, 20763−20771
Read Online

ACCESS | Metrics & More | Article Recommendations | Supporting Information

ABSTRACT: Excitonic effects caused by Coulomb interactions between electrons and holes play subtle and significant roles on photocatalysis, yet have been long ignored. Herein, porphyrinic covalent organic frameworks (COFs, specifically DhaTph-M), in the absence or presence of different metals in porphyrin centers, have been shown as ideal models to regulate excitonic effects. Remarkably, the incorporation of Zn^{2+} in the COF facilitates the conversion of singlet to triplet excitons, whereas the Ni^{2+} introduction promotes the dissociation of excitons to hot carriers under photoexcitation. Accordingly, the discriminative excitonic behavior of DhaTph-Zn and DhaTph-Ni enables the activation of O_2 to $^1O_2$ and $O_2^{\bullet-}$, respectively, under visible light irradiation, resulting in distinctly different activity and selectivity in photocatalytic terpinene oxidation. Benefiting from these results, DhaTph-Ni exhibits excellent photocatalytic activity in $O_2^{\bullet-}$-engaged hydroxylation of boronic acid, while DhaTph-Zn possesses superior performance in $^1O_2$-mediated selective oxidation of organic sulfides. This work provides in-depth insights into molecular oxygen activation and opens an avenue to the regulation of excitonic effects based on COFs.

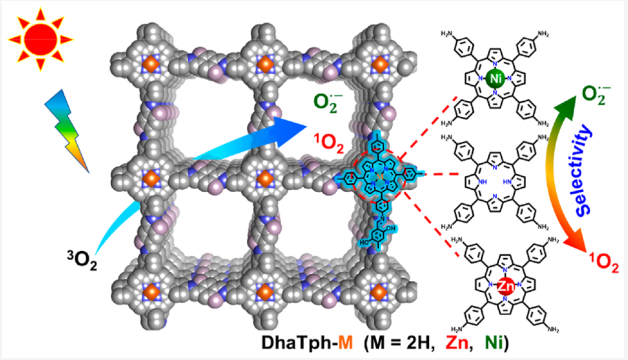

INTRODUCTION

The global energy and environmental issues raise unprecedented urgency on alternative clean and renewable energy supplies. Semiconductor-based photocatalysis, converting green and renewable solar energy into value-added chemicals and fuels, has captured great interests.[1−3] The separation of photogenerated carriers has been well accepted in photocatalysis.[4,5] Unfortunately, this well-established knowledge basis neglects the Coulomb interaction of electron−hole pairs, which is called excitonic effects and should be taken into account in some optical excitation processes, especially in strong exciton (electron−hole bound state) systems.[6,7] The neutral excitons and charge carriers are in a competitive relationship toward photocatalysis. The strong interaction in excitons readily causes exciton−exciton annihilation, which is detrimental to the generation of hot carriers.[8] Therefore, the charge separation and band structure optimizations, being long recognized as significant factors in photocatalysis, are incomplete when the competitive excitonic effects exist, which are able to give rise to distinct photocatalytic performance. In this context, it would be highly important and desired to gain deep insights into the excitonic aspects in photocatalysis.

Polymeric semiconductors known as "plastic optoelectronics" are promising photocatalysts due to their good efficiency and sustainability.[9−11] They actually fall into a class of strong exciton system given their generally low dielectric properties. Moreover, their exciton binding energy (E_b), a key parameter to evaluate the strength of exciton, is very high (typically >100 meV), much stronger than that of typical inorganic semiconductors.[12−15] As noted above, the strong Coulomb interaction of electron−hole pairs in polymeric photocatalysts impedes the dissociation of excitons to charge carriers, thereby suppressing the charge transfer processes and related photocatalytic efficiency.[16] Although this giant excitonic effect is unfavorable to charge transfer, it might promote some important energy transfer processes under photoexcitation, such as the conversion of O_2 to $^1O_2$ involving the activation of spin-triplet excitons.[16,17] Therefore, polymeric semiconductor might be a suitable model to investigate the role of the excitonic effects in specific reactions under photoexcitation. Unfortunately, there have been very limited studies on polymeric photocatalysts, where they are almost related to g-C_3N_4 or conjugated polymers.[12,18−21]

Despite the very helpful understanding of exciton behavior promoted by these studies, the lack of ordered structures in classical polymers is unfavorable to the precise fabrication and structural modification, posing challenges in accurate control

Received: September 10, 2020
Published: November 23, 2020

Downloaded via UNIV SCIENCE AND TECHNOLOGY CHINA on December 14, 2020 at 09:02:52 (UTC).
See https://pubs.acs.org/sharingguidelines for options on how to legitimately share published articles.

© 2020 American Chemical Society

https://dx.doi.org/10.1021/jacs.0c09727
J. Am. Chem. Soc. 2020, 142, 20763−20771

over excitons as well as disclosure of a clear relationship profile between excitonic effects and related properties. In light of this, the exploration of crystalline polymeric photocatalysts with well-defined and tunable structures would be desirable to achieve precise control of the exciton dissociation and transformation. To this end, covalent organic frameworks (COFs), a new class of crystalline polymers with tailorable structures,[22−37] would be ideal candidates, which greatly facilitate the regulation of the structures and excitonic effects. To our knowledge, there has yet been systematic investigation on excitonic effects for photocatalysis over COFs thus far.

Herein, the porphyrinic COFs, DhaTph-M in the absence or presence of different metal ions centered in the porphyrin linkers, have been rationally fabricated.[38−40] The metal-free COF presents the coexistence of excitons and charge carriers under irradiation. This balance is broken by incorporating different metal ions, significantly altering the behavior of excitons. Specifically, the Zn^{2+} in the porphyrin center can efficiently convert the singlet to triplet excitons and boost the energy transfer process, activating oxygen molecules to produce $^1O_2$. By contrast, the Ni^{2+} in the porphyrin center accelerates exciton dissociation to carriers and promotes the charge transfer process, generating $O_2^{\bullet-}$ from O_2 (Figure 1).

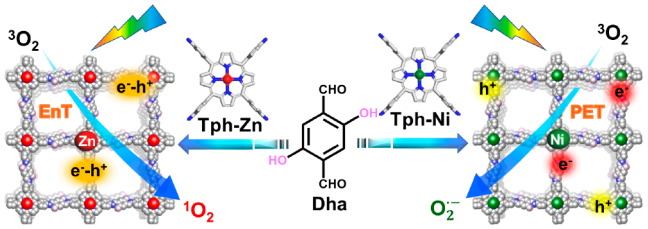

Figure 1. Synthesis and crystal structure of DhaTph-M (M = Zn and Ni) with different porphyrinic metal centers and diagram representation of their discriminative oxygen activation selectivity to $^1O_2$ and $O_2^{\bullet-}$ under visible light irradiation. EnT: energy transfer. PET: photoinduced electron transfer.

As a result, the oxidation of α-terpinene over DhaTph-Zn and DhaTph-Ni selectively produces ascaridole and *p*-cymene, respectively, under identical visible light irradiation conditions. In addition, selective oxidation of organic sulfides and hydroxylation of boronic acids can be intentionally promoted by DhaTph-Zn and DhaTph-Ni, respectively, based on the above understanding and regulation of excitonic effects.

RESULTS AND DISCUSSION

The DhaTph-M were synthesized via the Schiff base condensation between 2,5-dihydroxyterephthalaldehyde (Dha) and 5,10,15,20-tetrakis(4-aminophenyl)-21H, 23H-porphine or metalated derivatives (Tph-M; M = Ni and Zn) under solvothermal conditions.[39] The successful introduction of metal ions into the porphyrin center is confirmed by inductively coupled plasma atomic emission spectrometer (ICP-AES) and X-ray photoelectron spectroscopy (XPS) results (Figure S1 and Table S1). The structures of DhaTph-M are similar to the well-known COF-366 except for the introduction of OH group adjacent to the Schiff base linkage. The formation of a hydrogen bond (OH···N═C) would guarantee good crystallinity and stability under illumination.[38] From powder X-ray diffraction (XRD) profiles for all of the COFs (DhaTph-M), the introduction of metal ions in the center of the porphyrin does not disturb the crystallinity of COFs (Figure S2). The Fourier-transform infrared (FT-IR) spectrum for DhaTph-2H matches well with the previous report, indicating the successful formation of the imine linkages (Figure S3).[38] The BET surface area of DhaTph is calculated to be 1223 $m^2\ g^{-1}$, similar to those of DhaTph-M (M = Zn and Ni; Figures S4−S6). Compared with the organic linkers, all DhaTph-M exhibit extended light absorption to the near-infrared region thanks to the π electron delocalization, reflecting their good light harvesting ability (Figures S7 and S8). The energy levels for the COFs are calculated based on Mott−Schottky and Tauc plots (Figures S9−S11). The flat band positions (LUMO) of DhaTph-M (M = 2H, Zn, and Ni) determined from Mott−Schottky plots are −0.95, −0.89, and −1.06 V vs the normal hydrogen electrode (NHE, pH 6.8), respectively. Obviously, the LUMO potential of all these COFs is sufficiently negative for many photocatalytic reactions such as the reduction of O_2 to $O_2^{\bullet-}$ (−0.33 eV vs NHE).[41]

To explore the excitonic effects in COFs, photoluminescence measurements have been conducted. Compared with DhaTph-2H, the intensity of the prompt fluorescence spectra significantly reduces when Zn and Ni ions are residing in the porphyrin center, where the fluorescence of DhaTph-Ni is almost quenched, indicating the much accelerated charge transfer (Figures S12 and S13). The temperature-dependent steady-state fluorescence has been performed to evaluate the recombination type.[18] The fluorescence is usually generated by the charge carrier recombination or radiative decay of singlet excitons.[18] The recombination of charge carriers is more likely to be trapped by defects at low temperature, giving rise to a lower fluorescence intensity. However, both DhaTph-2H and DhaTph-Zn present increased fluorescence intensity at 223 K in reference to that at 298 K, indicating that the fluorescence might be produced by the decay of singlet excitons (Figure S14).

Phosphorescence stemmed from the emission of triplet excitons has been also examined to understand the efficiency of intersystem crossing (ISC), which is related to the process of transition from singlet to triplet state. In contrast to the fluorescence profiles (blue curve), the phosphorescence spectra (red curve) undergo red shift at a long decay time of 1 μs at 230 K (Figures 2a and 2b). The phosphorescence emission of DhaTph-2H exhibits two peaks at 674 and 709 nm in comparison to the fluorescence emission of 663 nm. The first peak might be the delayed fluorescence coming from the triplet excitons retransition back to the singlet state.[18] DhaTph-Zn shows a phosphorescence emission at 712 nm and fluorescence emission at 632 nm. The significant difference of the relative intensity between fluorescence and phosphorescence peaks from these two COFs shows that the proportion of phosphorescence emission by DhaTph-Zn is larger than that by DhaTph-2H, indicating that the addition of Zn(II) in the porphyrin center promotes the ISC process. To further explore the effect of different metal atoms in the porphyrin center, the electronic structures of related COFs have been studied by density-functional theory (DFT) calculations. As revealed by the density of states (DOS) profiles (Figures 2c,d and S15), the introduction of the Ni atom significantly enhances the DOS of valence band maximum (VBM), while the Zn atom takes a little bit of influence, in reference to DhaTph-2H. Therefore, more electrons in DhaTph-Ni can be photoexcited to the conduction band, promoting the electron transfer reactions. In addition, the electronic band structures of DhaTph-Ni and DhaTph-Zn

https://dx.doi.org/10.1021/jacs.0c09727
J. Am. Chem. Soc. 2020, 142, 20763−20771

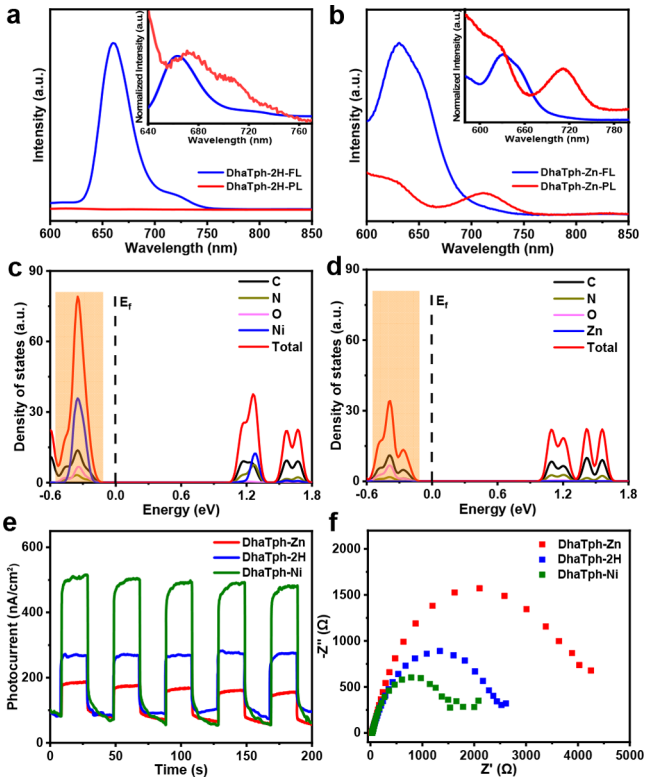

Figure 2. Steady-state prompt fluorescence (blue curves) and phosphorescence (red curves) spectra at 230 K (delay time 1 μs) for (a) DhaTph-2H and (b) DhaTph-Zn. Inset: normalized steady-state fluorescence and phosphorescence spectra. Calculated DOS profiles of (c) DhaTph-Ni and (d) DhaTph-Zn slabs (orange part represents the DOS around the VBM, E_f = Fermi level). (e) Photocurrent responses and (f) EIS Nyquist plots for DhaTph-M (M = 2H, Zn, and Ni).

were calculated (Figure S16). The increased number of the valence bands near the Fermi level in DhaTph-Ni reveals that more electrons can be excited, approving the results from the DOS calculation. This conclusion is further supported by the photocurrent and electrochemical impedance spectroscopy (EIS) results (Figure 2e,f). DhaTph-Ni exhibits the strongest photocurrent response and the lowest charge-transfer resistance among the three COFs due to the increased free charge carriers via accelerated exciton dissociation. In sharp contrast, the giant electron−hole interaction results in strong excitonic effect and greatly reduced free charge carriers in DhaTph-Zn.

To better understand distinct excitonic effects in DhaTph-M, their behaviors on molecular oxygen activation have been investigated. Generally, oxygen molecules can be activated to generate different reactive oxygen species (ROS), such as superoxide anion radical ($O_2^{\bullet-}$), hydrogen peroxide (H_2O_2), singlet oxygen ($^1O_2$), and hydroxyl radical (•OH).[42−50] Generally, electron transfer (via exciton dissociation) usually accounts for the production of $O_2^{\bullet-}$ and •OH while the energy transfer process where singlet excitons transform to triplet excitons and then react with ground state oxygen ($^3O_2$) is responsible for the $^1O_2$ generation.[51] Therefore, the excitonic effects in DhaTph-M are correlated with different ROS, which further affect the photocatalytic performance in O_2-engaged reactions. It is well established that porphyrin molecules are excellent photosensitizers for $^1O_2$ generation, which can be probed via the oxidation of α-terpinene toward ascaridole (Table 1).[52−54] As preliminary attempts, all homogeneous porphyrinic units in the absence or presence of the Zn/Ni

Table 1. Photocatalytic Oxidation of α-Terpinene over Different Catalysts in O_2 Atmosphere under Visible Light Irradiation[a]

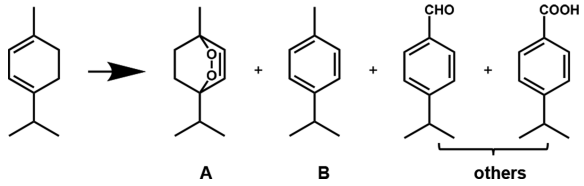

entry	catalyst	time (h)	conversion[b] (%)	selectivity[b] (%) A	B	others
1	Tph-2H	3	99	91	9	trace
2	Tph-Zn	3	99	93	7	trace
3	Tph-Ni	3	99	83	17	trace
4	DhaTph-Zn	4	99	85	15	trace
5	DhaTph-2H	4	97	70	28	2
6	DhaTph-Ni	6	76	7	81	12
7[c]	DhaTph-Zn	4	45	82	18	trace
8[c]	DhaTph-Ni	6	26	3	92	5
9[d]	DhaTph-Zn	4	trace			
10[d]	DhaTph-Ni	6	trace	trace	98	2
11	blank	6	15			
12[e]	DhaTph-Zn	4	trace			
13[e]	DhaTph-Ni	6	trace			

[a]Reaction conditions: catalyst (10 mg), α-terpinene (0.1 mmol), 3 mL of CH_3CN, 300 W Xe Lamp with visible light (λ > 420 nm), O_2 (1 atm). [b]Yield of products was analyzed by GC, and *n*-dodecane was used as the internal standard. [c]In air. [d]In N_2. [e]At 75 °C, without light.

center show very high activity and selectivity to α-terpinene (entries 1−3), supporting the key role of $^1O_2$ in the process. The oxidation of α-terpinene over porphyrinic COFs, DhaTph-M, has been then investigated in CH_3CN under O_2 atmosphere and visible-light irradiation to assess their ability to produce $^1O_2$. Among all of the COFs investigated, DhaTph-Zn possesses the highest catalytic activity (99%) and selectivity (85%) toward ascaridole under identical conditions (entry 4). The higher selectivity than DhaTph-2H demonstrates its better ability to produce $^1O_2$ (entry 5), given that the installation of Zn ions in the porphyrin center causes increased concentration of triplet excitons, as approved by the stronger phosphorescence emission (Figure 2b). In contrast, DhaTph-Ni exhibits as high as 93% *p*-cymene-based product (81% of *p*-cymene and a 12% of its further oxidized product), while only 7% of $^1O_2$-associated ascaridole is produced (entry 6). The discriminative product selectivity is attributed to different reaction paths with respective ROS generated.[48] The common feature in the reaction with different catalysts lies in that oxygen plays a central role. In the presence of DhaTph-M (M = Zn, Ni) catalysts, the reaction displays greatly reduced activity in air (entries 7 and 8) and becomes almost inactive in N_2 atmosphere (entries 9 and 10). The reaction gives a low activity (15%) and almost complete selectivity to *p*-cymene-based product in the absence of catalysts (entry 11), which is ascribed to the autoxidation of α-terpinene.[52] The replacement of light with heating at 75 °C does not reach any conversion (entries 12 and 13), demonstrating the indispensable role of light. All of the above results suggest that the strong electron−

https://dx.doi.org/10.1021/jacs.0c09727
J. Am. Chem. Soc. 2020, 142, 20763−20771

hole interaction in DhaTph-Zn and homogeneous Tph-M tends to induce energy transfer process, thereby giving the $^1O_2$ based products. In contrast, DhaTph-Ni promotes exciton dissociation, and accordingly charge carriers dominate the reaction with other ROS rather than $^1O_2$.

To further clarify the specific ROS produced by DhaTph-Zn and DhaTph-Ni, a series of 3,3′,5,5′-tetramethylbenzidine (TMB) oxidation experiments have been completed. The oxidation degree of TMB can be evaluated by monitoring the increasing absorbance peak at ~370 nm.[44] The results suggest that both DhaTph-Zn and DhaTph-Ni are able to oxidize TMB under visible-light irradiation, although the former displays a higher activity than DhaTph-Ni, similar to the above terpinene oxidation (Figure 3a,b). Various scavengers

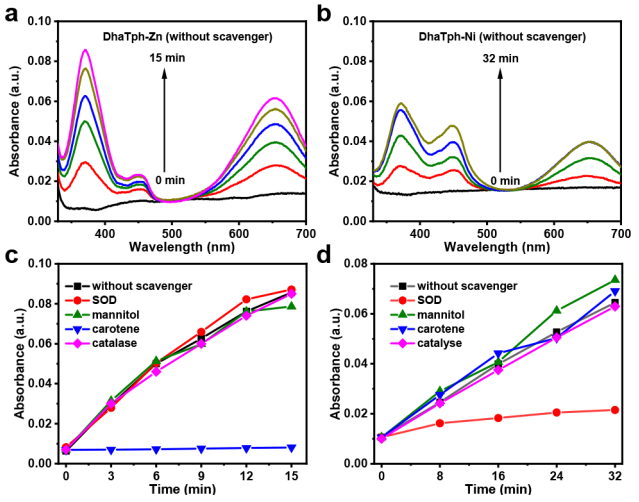

Figure 3. Time-dependent UV−vis absorption spectra recording TMB oxidation over (a) DhaTph-Zn and (b) DhaTph-Ni. UV−vis absorbance for TMB oxidation product monitored at 370 nm along with reaction time over (c) DhaTph-Zn and (d) DhaTph-Ni in the presence of different scavengers in O_2 atmosphere under visible light irradiation.

including carotene, mannite, superoxide dismutase (SOD), and catalase, which are the scavenger of $^1O_2$, •OH, $O_2^{\bullet-}$, and H_2O_2, respectively, have been introduced to investigate their respective influences (Figures S17 and S18). For DhaTph-Zn, carotene completely suppresses the conversion while the other scavengers make negligible influence, clearly indicating that $^1O_2$ being the ROS promotes the reaction (Figure 3c). In comparison, for DhaTph-Ni, the reaction rate is significantly inhibited by SOD rather than other scavengers (Figure 3d). The dominant species is reasonably inferred as $O_2^{\bullet-}$, pointing to the electron transfer behavior in DhaTph-Ni. Furthermore, nitro blue tetrazolium (NBT), which can be solely reduced by $O_2^{\bullet-}$,[41,55] has been examined with these two COFs (Figure S19). Time-resolved absorption spectra of NBT at 260 nm indicates that the $O_2^{\bullet-}$ generation rate by DhaTph-Ni is 16.3 times higher than that of DhaTph-Zn (Figure S20), highlighting the much greater ability of the former in the $O_2^{\bullet-}$ production. In addition, singlet oxygen sensor green (SOSG), which hardly reacts with ROS other than $^1O_2$,[44] is an ideal candidate to further verify the $^1O_2$ production (Figure S21). The reaction product between $^1O_2$ and SOSG gives a maxim fluorescence emission at ~525 nm. As a result, with DhaTph-Zn, the fluorescence signal at 525 nm is significant with increased irradiation time, clearly indicating the production of $^1O_2$ over DhaTph-Zn under visible light irradiation. In contrast, almost no peak at 525 nm can be observed with Dha-Tph-Ni under similar conditions.

Electron spin resonance (ESR) spectroscopy, recognized as the most convincing evidence to identify ROS, has been adopted to further distinguish different ROS generated over DhaTph-Ni and DhaTph-Zn. The 5,5-dimethyl-1-pyrroline-*N*-oxide (DMPO) is a radical trapping agent particularly for identifying $O_2^{\bullet-}$. DhaTph-Ni shows the typical signal of DMPO-OOH, further proving the generation of $O_2^{\bullet-}$ (Figure 4a). In sharp contrast, DhaTph-Zn gives negligible signals. On

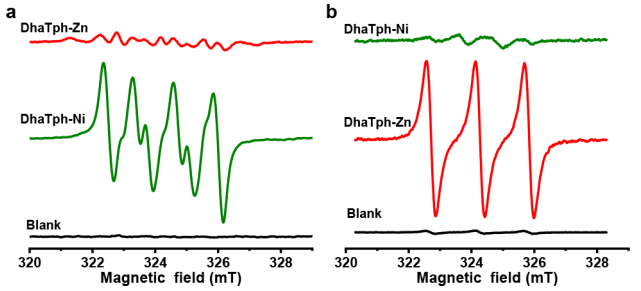

Figure 4. ESR spectra of (a) DhaTph-Ni and DhaTph-Zn in the presence of DMPO and (b) DhaTph-Ni and DhaTph-Zn in the presence of TEMP, in O_2 atmosphere under visible light irradiation.

the other hand, 2,2,6,6-tetramethylpiperidine (TEMP), a well-known $^1O_2$ probe, is selected to trap $^1O_2$ to generate stable nitroxide radical 2,2,6,6-tetramethylpiperidine-*N*-oxyl (TEMPO). The strong and characteristic 1:1:1 triplet ESR signal of TEMPO for DhaTph-Zn demonstrates the $^1O_2$ production (Figure 4b). However, the ignorable weak signal is observed for DhaTph-Ni. In addition, the ESR signals have also been collected after introducing particular scavengers, again unambiguously demonstrating that O_2 can be activated to $^1O_2$ and $O_2^{\bullet-}$ by DhaTph-Zn and DhaTph-Ni, respectively, under visible light irradiation (Figure S22).

From the above results, it is very clear that the excitonic effect is readily regulated by changing the porphyrinic metal centers in the COFs, which dominate the generation of specific ROS, $^1O_2$ and $O_2^{\bullet-}$, respectively, by energy transfer and charge transfer processes. This finding encourages us to investigate the specific reactions by taking advantage of the evolved ROS with the COFs. The photocatalytic hydroxylation of boronic acids, mainly promoted by $O_2^{\bullet-}$,[56−58] has been examined (Table 2). As expected, DhaTph-Ni, capable of activating O_2 to $O_2^{\bullet-}$, exhibits an excellent yield of 99% in 1.5 h with O_2 under visible irradiation (entry 1). The presence of triethylamine (TEA) would cause its reaction with holes to accelerate exciton dissociation and produce more $O_2^{\bullet-}$, promoting this reaction. By contrast, DhaTph-Zn, prone to convert O_2 to $^1O_2$, displays a much lower yield of 35% under identical conditions (entry 2). DhaTph-2H exhibits a moderate yield of 78% (entry 3), falling in between DhaTph-M (M = Ni, Zn). All porphyrin molecules, such as Tph-2H, Tph-Zn, and Tph-Ni also give low yields of 2%, 2%, and 10%, respectively, indicating their poor capability of exciton dissociation (entries 4−6). Control experiments confirm that this is a real photocatalytic process, in which photocatalyst (entry 7), O_2 (entry 8), and light irradiation (entry 9) are all essential elements for the reaction. The DhaTph-Ni exhibits excellent stability, and the reaction activity can be well retained after three cycles (entry 10 and

https://dx.doi.org/10.1021/jacs.0c09727
J. Am. Chem. Soc. 2020, 142, 20763−20771

Table 2. Photocatalytic Oxidative Hydroxylation of Phenylboronic Acid in the Absence or Presence of Different Catalysts[a]

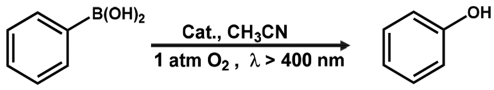

entry	catalyst	time (h)	yield[a] (%)
1	DhaTph-Ni	1.5	99
2	DhaTph-Zn	1.5	35
3	DhaTph-2H	1.5	78
4	Tph-2H	1.5	2
5	Tph-Ni	1.5	10
6	Tph-Zn	1.5	2
7	blank	6	trace
8[c]	DhaTph-Ni	6	trace
9[d]	DhaTph-Ni	6	trace
10[e]	DhaTph-Ni	1.5	95

[a]Reaction conditions: catalyst (10 mg), phenylboronic acid (0.1 mmol), 3 mL of CH_3CN, 50 μL of TEA, 300 W Xe Lamp with visible light (λ > 400 nm), O_2 (1 atm). [b]Yield of products was analyzed by GC, and *n*-dodecane was used as the internal standard. [c]In N_2. [d]Without light. [e]The 3rd run of the reaction.

Figure S23). In addition, several other phenylboronic acids substituted with electron-withdrawing and -rich groups have been investigated, and all results indicate the higher conversion over DhaTph-Ni than Dha-Tph-Zn (Table S2), further supporting the more favorable charge separation capability of the former.

For comparison, the oxidation of organic sulfides, where $^1O_2$ can selectively convert thioanisole to sulfoxide,[17,54] has been conducted to investigate the catalytic activity of DhaTph-Zn (Table 3). As expected, it exhibits a high conversion (82%)

Table 3. Photocatalytic Selective Oxidation of Thioanisole in the Absence or Presence of Different Catalysts[a]

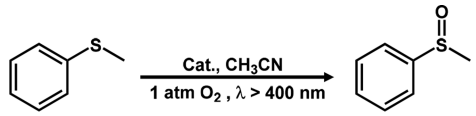

entry	catalyst	time (h)	con.[b] (%)	sel.[b] (%)
1	DhaTph-Zn	10	82	>99
2	DhaTph-Ni	10	20	>99
3	DhaTph-Ni	24	61	>99
4	DhaTph-2H	10	56	>99
5	blank	10	teace	
6[c]	DhaTph-Zn	10	trace	
7[d]	DhaTph-Zn	10	trace	
8[e]	DhaTph-Zn	10	80	>99

[a]Reaction conditions: catalyst (10 mg), thioanisole (0.05 mmol), 2 mL of CH_3CN and 1 mL of CH_3OH, 300 W Xe lamp with visible light (λ > 400 nm), O_2 (1 atm). [b]Yield of products was analyzed by GC, and *n*-dodecane was used as the internal standard. [c]In N_2. [d]Without light. [e]The 3rd run of the reaction.

and selectivity (>99%) to the desired monooxidized product, methyl phenyl sulfoxide, in 10 h with O_2 under visible light, indicating the high production of $^1O_2$ (entry 1). Although photooxygenation of sulfides also involves the $O_2^{\bullet-}$ and hole co-oxidation mechanism,[54] DhaTph-Ni, producing $O_2^{\bullet-}$ and holes, exhibits a low conversion of 20% only in 10 h and 61% in 24 h (entries 2 and 3). As expected, DhaTph-2H exhibits a moderate yield of 56% (entry 4). Control experiments are performed to confirm indispensability of photocatalyst (entry 5), O_2 (entry 6), and light irradiation (entry 7). After three cycles, the high activity and crystallinity of DhaTph-Zn are well maintained (entry 8 and Figure S24). The above two catalytic reactions apparently illustrate the significant role of excitonic effects in photocatalysis, where the rational design of photocatalysts is able to greatly boost the specific reaction process.

The generation of $O_2^{\bullet-}$ is assumed to be an electron transfer process. When DhaTph-Ni is excited by light, the excitons dissociate into charge carriers around the Ni centers due to the energetic disorders.[19] Then the electrons transport to O_2 molecules adsorbed on the Ni sites to afford $O_2^{\bullet-}$ (Figure 5a), a process extensively studied in the semiconductor-based

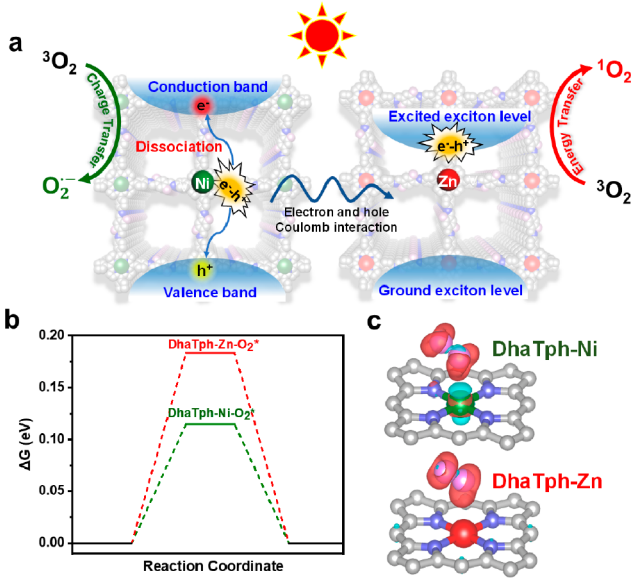

Figure 5. (a) Mechanism of photocatalytic molecular oxygen activation over DhaTph-Ni and DhaTph-Zn. (b) Free-energy diagram of O_2 adsorption on active metal sites in DhaTph-Ni and DhaTph-Zn. (c) Calculated charge density difference for DhaTph-Ni and DhaTph-Zn in the presence and absence of O_2 with the isosurfaces value of 0.0015 e/Å^3 (crimson and cyan represent charge accumulation and charge depletion, respectively).

photocatalytic systems.[59,60] Therefore, oxygen adsorption on the Ni sites is crucial for the electron transfer process to produce $O_2^{\bullet-}$. In contrast, the $^1O_2$ production tends to be an energy transfer process. Upon photoexcitation over DhaTph-Zn, the singlet excitons transform to triplet because of the strong diamagnetism with the d^{10} configuration of Zn^{2+}.[44] The triplet excitons are able to activate O_2 molecules in the ground state to $^1O_2$ by resonance energy transfer (Figure 5a). In this process, direct contact between oxygen and catalysts is not necessary, and it can take place via the dipole−dipole interactions or charge exchange between donor and acceptor.[61,62] Given the above understandings, adsorption energy between oxygen and the catalyst can be employed to evaluate the probability of electron transfer process. DFT calculations have been conducted to evaluate the adsorption energy between the catalysts and O_2 (Figures S25 and S26). Results suggest that the binding of O_2 on DhaTph-Ni is stronger (as indicated by adsorption free energy) than DhaTph-Zn, which

https://dx.doi.org/10.1021/jacs.0c09727
J. Am. Chem. Soc. 2020, 142, 20763−20771

reflects that electron transfer, where oxygen adsorption is crucial as indicated above, is a favorable process in DhaTph-Ni (Figure 5b). Excitons in DhaTph-Ni are easily dissociated into charge carriers around the Ni sites, where O_2 molecules are prone to be adsorbed, giving rise to the generation of $O_2^{\bullet-}$. Although O_2 molecules are difficult to be adsorbed onto DhaTph-Zn, the significantly increased concentration of triplet excitons enables energy transfer, which does not require direct contact, thereby producing singlet oxygen.

To further get deep insight into the above process, the calculated charge density difference for DhaTph-Ni (0.19 e) and DhaTph-Zn (0.15 e) in the presence and absence of O_2 suggests that more charges are transferred to O_2 over DhaTph-Ni than DhaTph-Zn (Figure 5c and Table S3).[63] Especially, the depletion of 0.07 e in the Ni center in reference to 0 e in the Zn center clearly demonstrates that the Ni^{2+} in the porphyrin center is prone to promote electron transfer to O_2 for the production of $O_2^{\bullet-}$, in good agreement with the above results.

CONCLUSIONS

In summary, the porphyrinic COFs involving diverse metal ions, DhaTph-M, have been synthesized and exhibit distinctly different excitonic effects, the regulation of which on COF photocatalysis has been systematically investigated for the first time. While the introduction of Zn^{2+} in the COF gives rise to the increase of triplet excitons, evidenced by sound phosphorescence intensity, the Ni^{2+} promotes exciton dissociation to charge carriers, as jointly demonstrated by increased DOS of VBM and photoelectrochemical results. In line with the above results, the oxidation of α-terpinene in O_2 over DhaTph-M affords distinctly different products as different ROS are evolved with these COFs. The results have been multiply confirmed by TMB oxidation, NBT reduction and EPR spectra, unambiguously demonstrating that the $^1O_2$ production by DhaTph-Zn while the generation of $O_2^{\bullet-}$ by DhaTph-Ni are preferred via the oxygen activation under light irradiation. With this knowledge on selective oxygen activation in mind, the particularly $O_2^{\bullet-}$ and $^1O_2$-involved catalytic reactions have been rationally promoted with the help of DhaTph-Ni and DhaTph-Zn, respectively. This work not only sheds new light on molecular oxygen activation by porphyrinic COFs but also provides deep insights into the regulation of excitonic effects toward improved photocatalysis.

MATERIALS AND METHODS

Materials and Equipment. All chemicals were purchased from commercial suppliers. XRD were collected on a Japan Rigaku Miniflex 600 rotation anode X-ray diffractometer equipped with graphite monochromatized Cu Kα radiation (λ = 1.54 Å). The UV−vis absorption spectra were recorded on a Shimadzu UV-3600 Plus in the wavelength range of 200−3600 nm. Nitrogen sorption isotherms were measured using a Micromeritics ASAP 2020 system at 77 K. Prior to N_2 sorption measurement, the samples were preactivated with supercritical carbon dioxide. The ICP-AES results were taken on Thermo scientific iCAP 7400 to confirm the metal contents. The XPS measurements were performed by a Kratos Axis Supra$^+$ high-performance electron spectrometer using monochromatized Al Kα ($h\nu$ = 1486.6 eV) as the excitation source. The catalytic reaction products were identified and analyzed by using a Shimadzu gas chromatograph (GC-2010 Plus with a 0.25 mm × 30 m Rtx-5 capillary column). The products were determined by using the Agilent technologies 7890A GC and a mass spectrometer Agilent technologies 5975C as detector. The light irradiation was obtained by 300 W xenon lamp (LX300F, Japan). Electron spin resonance spectra (ESR) were collected on a JES-FA200 electron paramagnetic resonance spectrometer under visible-light irradiation.

Synthesis of DhaTph-M (M = 2H, Ni). The COF sythesis was performed following previous reports with some minor modifications.[37] Typically, TPh-M (M = 2H or Ni, 0.04 mmol) and Dha (0.08 mmol) in an mixed solvent of *o*-dichlorobenzene/*n*-butanol/6 M HAC (1:1:0.2 mL) were degassed in a glass tube by liquid nitrogen. The tube was sealed off and heated at 120 °C for 3 or more days. The solid was isolated by centrifugation and washed with THF and acetone until the supernatant is colorless. Then the samples were further dried overnight at 393 K under vacuum for further use.

Synthesis of DhaTph-Zn. The synthetic procedure of DhaTph-Zn was similar to that of DhaTPh-M (M = 2H, Ni) except for *o*-dichlorobenzene/*n*-butanol/6 M HAC (1:1:0.25 mL) and the amount of Tph-Zn (0.025 mmol) and Dha (0.05 mmol).

Photoelectrochemical Measurements. Photocurrent measurements were conducted with a CHI 760E electrochemical workstation (Chenhua Instrument, Shanghai, China) in a standard three-electrode system with the photocatalyst-coated FTO as the working electrode, Pt plate as the counter electrode, and an Ag/AgCl as a reference electrode. A 300 W xenon lamp with a UV cutoff filter (>380 nm) was used as the light source. EIS was performed with a Zahner Zennium electrochemical workstation in a conventional three electrode cell, using a Pt plate as the counter electrode and Ag/AgCl electrode as the reference electrode. The electrolyte was a 0.1 M Na_2SO_4 solution. The 2 mg of catalyst was added into 1 mL of CH_3OH and 10 μL of Nafion mixed solution. Then a 100 μL suspension was dropped on the surface of a FTO glass and dried at room temperature for photocurrent measurements, and the signals were recorded under chopped light at 0.5 V. EIS was performed with a 30 μL suspension on the working electrode in a frequency range from 10^{-1} to 10^5 Hz with a bias potential of −1.5 V.

TMB Oxidation Measurements. Typically, 5 mg of TMB was dissolved with 1 mL of H_2O and 2 mL of HAc/NaAc buffer solution (0.2:0.2 M). A total of 200 μL of COF aqueous solution (5 mg/mL) was then added into the mixture solution with O_2 bubbling under visible light irradiation. The samples were taken at different time intervals for UV−vis measurements. In order to verify the specific ROS, various scavengers were added into the TMB solution before the light irradiation: carotene (10 mg), mannite (2 mg), catalase (2 mg), and superoxide dismutase (SOD, 200 μL), respectively.

NBT Reduction Measurements. Typically, 3.5 mg of nitro blue tetrazolium (NBT) was ultrasonically dispersed in 1 mL of phosphate buffer (pH 7). Then 3 mg of Dha-Tph-M (Zn, Ni) was ultrasonically dispersed in another 1 mL of phosphate buffer (pH 7). The above two solutions were mixed with O_2 bubbling under visible light irradiation. At different time intervals the samples were taken for further UV−vis measurements.

ESR Detection. The ROS generated by COFs have been detected by ESR in the presence of DMPO and TEMP, respectively. Typically, 30 μL DMPO or TEMP in 1 mL MeOH was mixed with 0.5 mL of COF/MeOH suspension (2 mg/2 mL). The formed mixture (300−400 μL) was added into the ESR tube. ESR measurements were carried out during the light irradiation with a 500 W xenon lamp (λ > 380 nm) under the air conditions.

General Procedure for Photocatalytic Oxidation of α-Terpinene. Typically, 10 mg of COFs was dispersed in 3 mL of CH_3CN, followed by the addition of 0.1 mmol of α-terpinene in a two-neck flask (10 mL). The reaction was carried out at ambient temperature with O_2 bubbling under illumination with a 300 W Xe lamp (λ > 420 nm) and magnetic stirring. Upon reaction completion, the reaction solution was centrifuged. Then, the conversion and selectivity were quantified by gas chromatography and the products were confirmed by GC-MS. The mass of porphyrin linkers was calculated based on the number of equivalents of Tph units in DhaTph-M.

General Procedure for Photocatalytic Hydroxylation of Boronic Acids and Selective Oxidation of Thioanisole. Typically, 10 mg of COFs was dispersed in 3 mL of CH_3CN,

https://dx.doi.org/10.1021/jacs.0c09727
J. Am. Chem. Soc. 2020, 142, 20763−20771

followed by the addition of 0.1 mmol of boronic acids and 50 μL of TEA in a 10 mL reaction tube equipped with a rubber septum. Prior to the reaction, the tube was filled with O_2 by three freeze−pump−thaw. The reaction was carried out at ambient temperature under visible light irradiation with a 300 W Xe lamp (λ > 400 nm) and magnetic stirring. Upon reaction completion, the reaction solution was centrifuged. Then, the conversion and selectivity were quantified by gas chromatography, and the products were confirmed by GC-MS. The mass of porphyrin linkers was calculated based on the number of equivalents of Tph units in DhaTph-M. Recycling experiments were performed by the following procedure: The solution after reaction was centrifuged and washed with CH_3CN 2 times, and then the catalyst was reused for a subsequent run with fresh boronic acid substrate (0.1 mmol), 50 μL of TEA, and 3 mL of CH_3CN under the aforementioned conditions. Selective oxidation of thioanisole is similar to hydroxylation of boronic acids except for 2 mL CH_3CN and 1 mL CH_3OH with the addition of 0.05 mmol of thioanisole.

DFT Calculations. The DFT calculations were performed with the VASP 5.4.1 program. The geometry optimization and electronic properties of the periodic structures were performed using the projector augmented wave (PAW) method implemented in the Vienna ab initio simulation package (VASP) code.[64] The generalized gradient approximation (GGA) functional to the exchange-correction functional, of Perdew−Burke−Ernzerhof (PBE) form with vdW corrections (VDW-DFT) was adopted in our calculations.[65] The electron wave function was expanded using plane waves with an energy cutoff of 400 eV. The lattice parameters were $a = b = 25.6$ Å and $\gamma = 60°$. A vacuum region about 20 Å to the surface was added to ensure decoupling between the next slabs. Then, 1 × 1 × 1 Gamma centered k-points were adopted for the cell in the Gibbs free energy calculation. The convergence standards of energy and force were selected as 10^{-5} eV and 0.05 eV/Å, respectively. During the calculation, all of the atoms are relaxed.

■ ASSOCIATED CONTENT

Supporting Information

The Supporting Information is available free of charge at https://pubs.acs.org/doi/10.1021/jacs.0c09727.

Additional figures mentioned in the text and details on ligand preparation, characterization data, and figures (PDF)

■ AUTHOR INFORMATION

Corresponding Author

Hai-Long Jiang − *Hefei National Laboratory for Physical Sciences at the Microscale, CAS Key Laboratory of Soft Matter Chemistry, Department of Chemistry, University of Science and Technology of China, Hefei, Anhui 230026, P.R. China;* orcid.org/0000-0002-2975-7977; Email: jianglab@ustc.edu.cn

Authors

Yunyang Qian − *Hefei National Laboratory for Physical Sciences at the Microscale, CAS Key Laboratory of Soft Matter Chemistry, Department of Chemistry, University of Science and Technology of China, Hefei, Anhui 230026, P.R. China*

Dandan Li − *Institutes of Physics Science and Information Technology, Anhui University, Hefei 230601, P.R. China;* orcid.org/0000-0002-3504-8739

Yulan Han − *Hefei National Laboratory for Physical Sciences at the Microscale, CAS Key Laboratory of Soft Matter Chemistry, Department of Chemistry, University of Science and Technology of China, Hefei, Anhui 230026, P.R. China*

Complete contact information is available at: https://pubs.acs.org/10.1021/jacs.0c09727

Notes

The authors declare no competing financial interest.

■ ACKNOWLEDGMENTS

This work is supported by the NSFC (21725101, 21673213, and 21521001). The calculations in this work are supported by the Supercomputing Center of University of Science and Technology of China.

■ REFERENCES

(1) Cook, T. R.; Dogutan, D. K.; Reece, S. Y.; Surendranath, Y.; Teets, T. S.; Nocera, D. G. Solar energy supply and storage for the legacy and nonlegacy worlds. *Chem. Rev.* **2010**, *110*, 6474−6502.

(2) Wang, H.; Zhu, Q.-L.; Zou, R.; Xu, Q. Metal-organic frameworks for energy applications. *Chem.* **2017**, *2*, 52−80.

(3) Zhang, S.; Cheng, G.; Guo, L.; Wang, N.; Tan, B.; Jin, S. Strong-base-assisted synthesis of a crystalline covalent triazine framework with high hydrophilicity via benzylamine monomer for photocatalytic water splitting. *Angew. Chem., Int. Ed.* **2020**, *59*, 6007−6014.

(4) Chen, X.; Shen, S.; Guo, L.; Mao, S. S. Semiconductor-based photocatalytic hydrogen generation. *Chem. Rev.* **2010**, *110*, 6503−6570.

(5) Serpone, N.; Emeline, A. V. Semiconductor photocatalysis-past, present, and future outlook. *J. Phys. Chem. Lett.* **2012**, *3*, 673−677.

(6) Herbst, J.; Lowy, D.; Watson, R. Band-structure modifications due to photogenerated carriers in a GaAs/AlxGa1-xAs heterostructure. *Phys. Rev. B* **1972**, *6*, 1913−1924.

(7) Cao, Y.; Parker, I. D.; Yu, G.; Zhang, C.; Heeger, A. J. Improved quantum efficiency for electroluminescence in semiconducting polymers. *Nature* **1999**, *397*, 414.

(8) Ma, Y. Z.; Valkunas, L.; Dexheimer, S. L.; Bachilo, S. M.; Fleming, G. R. Femtosecond spectroscopy of optical excitations in single-walled carbon nanotubes: evidence for exciton-exciton annihilation. *Phys. Rev. Lett.* **2005**, *94*, 157402.

(9) Wang, X.; Maeda, K.; Chen, X.; Takanabe, K.; Domen, K.; Hou, Y.; Fu, X.; Antonietti, M. Polymer semiconductors for artificial photosynthesis: hydrogen evolution by mesoporous graphitic carbon nitride with visible light. *J. Am. Chem. Soc.* **2009**, *131*, 1680−1681.

(10) Wang, Y.; Vogel, A.; Sachs, M.; Sprick, R. S.; Wilbraham, L.; Moniz, S. J. A.; Godin, R.; Zwijnenburg, M. A.; Durrant, J. R.; Cooper, A. I.; Tang, J. Current understanding and challenges of solar-driven hydrogen generation using polymeric photocatalysts. *Nat. Energy* **2019**, *4*, 746−760.

(11) Yu, M.; Dong, R.; Feng, X. Two-dimensional carbon-rich conjugated frameworks for electrochemical energy applications. *J. Am. Chem. Soc.* **2020**, *142*, 12903−12915.

(12) Lan, Z. A.; Zhang, G.; Chen, X.; Zhang, Y.; Zhang, K. A. I.; Wang, X. Reducing the exciton binding energy of donor-acceptor-based conjugated polymers to promote charge-induced reactions. *Angew. Chem., Int. Ed.* **2019**, *58*, 10236−10240.

(13) Heeger, A. J. Semiconducting polymers: the third generation. *Chem. Soc. Rev.* **2010**, *39*, 2354−2371.

(14) Kim, T. W.; Jun, S.; Ha, Y.; Yadav, R. K.; Kumar, A.; Yoo, C.-Y.; Oh, I.; Lim, H.-K.; Shin, J. W.; Ryoo, R.; Kim, H.; Kim, J.; Baeg, J.-O.; Ihee, H. Ultrafast charge transfer coupled with lattice phonons in two-dimensional covalent organic frameworks. *Nat. Commun.* **2019**, *10*, 1873.

(15) Flanders, N. C.; Kirschner, M. S.; Kim, P.; Fauvell, T. J.; Evans, A. M.; Helweh, W.; Spencer, A. P.; Schaller, R. D.; Dichtel, W. R.; Chen, L. X. Large exciton diffusion coefficients in two dimensional covalent organic frameworks with different domain sizes revealed by ultrafast exciton dynamics. *J. Am. Chem. Soc.* **2020**, *142*, 14957−14965.

(16) Schweitzer, C.; Schmidt, R. Physical mechanisms of generation and deactivation of singlet oxygen. *Chem. Rev.* **2003**, *103*, 1685.

(17) Wang, H.; Jiang, S.; Chen, S.; Li, D.; Zhang, X.; Shao, W.; Sun, X.; Xie, J.; Zhao, Z.; Zhang, Q.; Tian, Y.; Xie, Y. Enhanced singlet oxygen generation in oxidized graphitic carbon nitride for organic synthesis. *Adv. Mater.* **2016**, *28*, 6940−6945.
(18) Wang, H.; Jiang, S.; Chen, S.; Zhang, X.; Shao, W.; Sun, X.; Zhao, Z.; Zhang, Q.; Luo, Y.; Xie, Y. Insights into the excitonic processes in polymeric photocatalysts. *Chem. Sci.* **2017**, *8*, 4087−4092.
(19) Wang, H.; Sun, X.; Li, D.; Zhang, X.; Chen, S.; Shao, W.; Tian, Y.; Xie, Y. Boosting hot-electron generation: exciton dissociation at the order-disorder interfaces in polymeric photocatalysts. *J. Am. Chem. Soc.* **2017**, *139*, 2468−2473.
(20) Zhang, G.; Li, G.; Lan, Z. A.; Lin, L.; Savateev, A.; Heil, T.; Zafeiratos, S.; Wang, X.; Antonietti, M. Optimizing optical absorption, exciton dissociation, and charge transfer of a polymeric carbon nitride with ultrahigh solar hydrogen production activity. *Angew. Chem., Int. Ed.* **2017**, *56*, 13445−13449.
(21) Sachs, M.; Sprick, R. S.; Pearce, D.; Hillman, S. A. J.; Monti, A.; Guilbert, A. A. Y.; Brownbill, N. J.; Dimitrov, S.; Shi, X.; Blanc, F.; Zwijnenburg, M. A.; Nelson, J.; Durrant, J. R.; Cooper, A. I. Understanding structure-activity relationships in linear polymer photocatalysts for hydrogen evolution. *Nat. Commun.* **2018**, *9*, 4968.
(22) Waller, P. J.; Gándara, F.; Yaghi, O. M. Chemistry of covalent organic frameworks. *Acc. Chem. Res.* **2015**, *48*, 3053−3063.
(23) Diercks, C. S.; Yaghi, O. M. The atom, the molecule, and the covalent organic framework. *Science* **2017**, *355*, 923.
(24) Geng, K.; He, T.; Liu, R.; Dalapati, S.; Tan, K. T.; Li, Z.; Tao, S.; Gong, Y.; Jiang, Q.; Jiang, D. Covalent organic frameworks: design, synthesis, and functions. *Chem. Rev.* **2020**, *120*, 8814−8933.
(25) Yusran, Y.; Guan, X.; Li, H.; Fang, Q.; Qiu, S. Postsynthetic functionalization of covalent organic frameworks. *Natl. Sci. Rev.* **2020**, *7*, 170−190.
(26) Wang, Z.; Zhang, S.; Chen, Y.; Zhang, Z.; Ma, S. Covalent organic frameworks for separation applications. *Chem. Soc. Rev.* **2020**, *49*, 708−735.
(27) Kandambeth, S.; Dey, K.; Banerjee, R. Covalent organic frameworks: chemistry beyond the structure. *J. Am. Chem. Soc.* **2019**, *141*, 1807−1822.
(28) Kang, X.; Wu, X.; Han, X.; Yuan, C.; Liu, Y.; Cui, Y. Rational synthesis of interpenetrated 3D covalent organic frameworks for asymmetric photocatalysis. *Chem. Sci.* **2020**, *11*, 1494−1502.
(29) Wang, G.-B.; Li, S.; Yan, C.-X.; Zhu, F.-C.; Lin, Q.-Q.; Xie, K.-H.; Geng, Y.; Dong, Y.-B. Covalent organic frameworks: emerging high-performance platforms for efficient photocatalytic applications. *J. Mater. Chem. A* **2020**, *8*, 6957−6983.
(30) Liang, R.-R.; Jiang, S.-Y.; A, R.-H.; Zhao, X. Two-dimensional covalent organic frameworks with hierarchical porosity. *Chem. Soc. Rev.* **2020**, *49*, 3920.
(31) Yang, S.; Hu, W.; Zhang, X.; He, P.; Pattengale, B.; Liu, C.; Cendejas, M.; Hermans, I.; Zhang, X.; Zhang, J.; Huang, J. 2D covalent organic frameworks as intrinsic photocatalysts for visible light-driven CO_2 reduction. *J. Am. Chem. Soc.* **2018**, *140*, 14614.
(32) Biswal, B. P.; Vignolo-Gonzalez, H. A.; Banerjee, T.; Grunenberg, L.; Savasci, G.; Gottschling, K.; Nuss, J.; Ochsenfeld, C.; Lotsch, B. V. Sustained solar H_2 evolution from a thiazolo[5,4-d]thiazole-bridged covalent organic framework and nickel-thiolate cluster in water. *J. Am. Chem. Soc.* **2019**, *141*, 11082−11092.
(33) Lu, M.; Liu, J.; Li, Q.; Zhang, M.; Liu, M.; Wang, J.-L.; Yuan, D.-Q.; Lan, Y.-Q. Rational design of crystalline covalent organic frameworks for efficient CO_2 photoreduction with H_2O. *Angew. Chem., Int. Ed.* **2019**, *58*, 12392−12397.
(34) Miao, Z.; Liu, G.; Cui, Y.; Liu, Z.; Li, J.; Han, F.; Liu, Y.; Sun, X.; Gong, X.; Zhai, Y.; Zhao, Y.; Zeng, Y. A novel strategy for the construction of covalent organic frameworks from nonporous covalent organic polymers. *Angew. Chem., Int. Ed.* **2019**, *58*, 4906.
(35) Kang, C.; Zhang, Z.; Wee, V.; Usadi, A. K.; Calabro, D. C.; Baugh, L. S.; Wang, S.; Wang, Y.; Zhao, D. Interlayer shifting in two-dimensional covalent organic frameworks. *J. Am. Chem. Soc.* **2020**, *142* (30), 12995−13002.
(36) Pachfule, P.; Acharjya, A.; Roeser, J.; Langenhahn, T.; Schwarze, M.; Schomacker, R.; Thomas, A.; Schmidt, J. Diacetylene functionalized covalent organic framework (COF) for photocatalytic hydrogen generation. *J. Am. Chem. Soc.* **2018**, *140*, 1423−1427.
(37) Zhong, W.; Sa, R.; Li, L.; He, Y.; Li, L.; Bi, J.; Zhuang, Z.; Yu, Y.; Zou, Z. A covalent organic framework bearing single Ni sites as a synergistic photocatalyst for selective photoreduction of CO_2 to CO. *J. Am. Chem. Soc.* **2019**, *141*, 7615−7621.
(38) Kandambeth, S.; Shinde, D. B.; Panda, M. K.; Lukose, B.; Heine, T.; Banerjee, R. Enhancement of chemical stability and crystallinity in porphyrin-containing covalent organic frameworks by intramolecular hydrogen bonds. *Angew. Chem., Int. Ed.* **2013**, *52*, 13052−13056.
(39) Chen, X.; Addicoat, M.; Jin, E.; Zhai, L.; Xu, H.; Huang, N.; Guo, Z.; Liu, L.; Irle, S.; Jiang, D. Locking covalent organic frameworks with hydrogen bonds: general and remarkable effects on crystalline structure, physical properties, and photochemical activity. *J. Am. Chem. Soc.* **2015**, *137*, 3241−3247.
(40) Diercks, C. S.; Lin, S.; Kornienko, N.; Kapustin, E. A.; Nichols, E. M.; Zhu, C.; Zhao, Y.; Chang, C. J.; Yaghi, O. M. Reticular electronic tuning of porphyrin active sites in covalent organic frameworks for electrocatalytic carbon dioxide reduction. *J. Am. Chem. Soc.* **2018**, *140*, 1116−1122.
(41) Nosaka, Y.; Nosaka, A. Y. Generation and detection of reactive oxygen species in photocatalysis. *Chem. Rev.* **2017**, *117*, 11302−11336.
(42) Wei, P.-F.; Qi, M.-Z.; Wang, Z.-P.; Ding, S.-Y.; Yu, W.; Liu, Q.; Wang, L.-K.; Wang, H.-Z.; An, W.-K.; Wang, W. Benzoxazole-linked ultrastable covalent organic frameworks for photocatalysis. *J. Am. Chem. Soc.* **2018**, *140*, 4623−4631.
(43) Meng, Y.; Luo, Y.; Shi, J.-L.; Ding, H.; Lang, X.; Chen, W.; Zheng, A.; Sun, J.; Wang, C. 2D and 3D porphyrinic covalent organic frameworks: the influence of dimensionality on functionality. *Angew. Chem., Int. Ed.* **2020**, *59*, 3624−3629.
(44) Chen, Y.-Z.; Wang, Z. U.; Wang, H.; Lu, J.; Yu, S.-H.; Jiang, H.-L. Singlet oxygen-engaged selective photo-oxidation over Pt nanocrystals/porphyrinic MOF: the roles of photothermal effect and Pt electronic state. *J. Am. Chem. Soc.* **2017**, *139*, 2035−2044.
(45) Xu, C.; Pan, Y.; Wan, G.; Liu, H.; Wang, L.; Zhou, H.; Yu, S.-H.; Jiang, H.-L. Turning on visible-Light photocatalytic C-H oxidation over metal-organic frameworks by introducing metal-to-cluster charge transfer. *J. Am. Chem. Soc.* **2019**, *141*, 19110−19117.
(46) Li, S.; Li, L.; Li, Y.; Dai, L.; Liu, C.; Liu, Y.; Li, J.; Lv, J.; Li, P.; Wang, B. Fully conjugated donor-acceptor covalent organic frameworks for photocatalytic oxidative amine coupling and thioamide cyclization. *ACS Catal.* **2020**, *10* (15), 8717−8726.
(47) Xu, C.; Liu, H.; Li, D.; Su, J.-H.; Jiang, H.-L. Direct evidence of charge separation in a metal-organic framework: efficient and selective photocatalytic oxidative coupling of amines via charge and energy transfer. *Chem. Sci.* **2018**, *9*, 3152−3158.
(48) Liang, X.; Guo, Z.; Wei, H.; Liu, X.; Lv, H.; Xing, H. Selective photooxidation of sulfides mediated by singlet oxygen using visible light-responsive coordination polymers. *Chem. Commun.* **2018**, *54*, 13002−13005.
(49) Wei, H.; Guo, Z.; Liang, X.; Chen, P.; Liu, H.; Xing, H. Selective photooxidation of amines and sulfides triggered by a superoxide radical using a novel visible-light-responsive metal organic framework. *ACS Appl. Mater. Interfaces* **2019**, *11*, 3016−3023.
(50) Liu, H.; Guo, Z.; Lv, H.; Liu, X.; Che, Y.; Mei, Y.; Bai, R.; Chi, Y.; Xing, H. Visible-light-driven self-coupling and oxidative dehydrogenation of amines to imines via a Mn(II)-based coordination polymer. *Inorg. Chem. Front.* **2020**, *7*, 1016−1025.
(51) Hao, W.; Chen, D.; Li, Y.; Yang, Z.; Xing, G.; Li, J.; Chen, L. Facile synthesis of porphyrin based covalent organic frameworks via an A_2B_2 monomer for highly efficient heterogeneous catalysis. *Chem. Mater.* **2019**, *31*, 8100−8105.
(52) Ronzani, F.; Costarramone, N.; Blanc, S.; Benabbou, A. K.; Bechec, M. L.; Pigot, T.; Oelgemöller, M.; Lacombe, S. Visible-light photosensitized oxidation of α-terpinene using novel silica-supported

https://dx.doi.org/10.1021/jacs.0c09727
J. Am. Chem. Soc. 2020, 142, 20763−20771

sensitizers: photooxygenation vs. photodehydrogenation. *J. Catal.* **2013**, *303*, 164−174.
(53) Tobin, J. M.; McCabe, T. J. D.; Prentice, A. W.; Holzer, S.; Lloyd, G. O.; Paterson, M. J.; Arrighi, V.; Cormack, P. A. G.; Vilela, F. Polymer-supported photosensitizers for oxidative organic transformations in flow and under visible light irradiation. *ACS Catal.* **2017**, *7*, 4602−4612.
(54) Wang, S.; Sun, Q.; Chen, W.; Tang, Y.; Aguila, B.; Pan, Y.; Zheng, A.; Yang, Z.; Wojtas, L.; Ma, S.; Xiao, F.-S. Programming Covalent Organic Frameworks for Photocatalysis: Investigation of Chemical and Structural Variations. *Matter* **2020**, *2*, 416−427.
(55) Huang, H.; Han, X.; Li, X.; Wang, S.; Chu, P. K.; Zhang, Y. Fabrication of multiple heterojunctions with tunable visible-light-active photocatalytic reactivity in BiOBr-BiOI full-range composites based on microstructure modulation and band structures. *ACS Appl. Mater. Interfaces* **2015**, *7*, 482−492.
(56) Pitre, S. P.; McTiernan, C. D.; Ismaili, H.; Scaiano, J. C. Mechanistic insights and kinetic analysis for the oxidative hydroxylation of arylboronic acids by visible light photoredox catalysis: a metal-free alternative. *J. Am. Chem. Soc.* **2013**, *135*, 13286−13289.
(57) Johnson, J. A.; Luo, J.; Zhang, X.; Chen, Y.-S.; Morton, M. D.; Echeverría, E.; Torres, F. E.; Zhang, J. Porphyrin-metalation-mediated tuning of photoredox catalytic Properties in metal-organic frameworks. *ACS Catal.* **2015**, *5*, 5283−5291.
(58) Bi, S.; Thiruvengadam, P.; Wei, S.; Zhang, W.; Zhang, F.; Gao, L.; Xu, J.; Wu, D.; Chen, J.-S.; Zhang, F. Vinylene-bridged two-dimensional covalent organic frameworks via Knoevenagel condensation of tricyanomesitylene. *J. Am. Chem. Soc.* **2020**, *142*, 11893−11900.
(59) Li, R.; Weng, Y.; Zhou, X.; Wang, X.; Mi, Y.; Chong, R.; Han, H.; Li, C. Achieving overall water splitting using titanium dioxide-based photocatalysts of different phases. *Energy Environ. Sci.* **2015**, *8*, 2377−2382.
(60) Zhang, P.; Tong, Y.; Liu, Y.; Vequizo, J. J. M.; Sun, H.; Yang, C.; Yamakata, A.; Fan, F.; Lin, W.; Wang, X.; Choi, W. Heteroatom dopants promote two-electron O_2 reduction for photocatalytic production of H_2O_2 on polymeric carbon nitride. *Angew. Chem., Int. Ed.* **2020**, *59*, 16209−16217.
(61) Cao, L.; Lin, Z.; Shi, W.; Wang, Z.; Zhang, C.; Hu, X.; Wang, C.; Lin, W. Exciton migration and amplified quenching on two-dimensional metal-organic layers. *J. Am. Chem. Soc.* **2017**, *139*, 7020−7029.
(62) Haldar, R.; Jakoby, M.; Mazel, A.; Zhang, Q.; Welle, A.; Mohamed, T.; Krolla, P.; Wenzel, W.; Diring, S.; Odobel, F.; Richards, B. S.; Howard, I. A.; Wöll, C. Anisotropic energy transfer in crystalline chromophore assemblies. *Nat. Commun.* **2018**, *9*, 4322.
(63) Wang, S.; Hai, X.; Ding, X.; Jin, S.; Xiang, Y.; Wang, P.; Jiang, B.; Ichihara, F.; Oshikiri, M.; Meng, X.; Li, Y.; Matsuda, W.; Ma, J.; Seki, S.; Wang, X.; Huang, H.; Wada, Y.; Chen, H.; Ye, J. Intermolecular cascaded π-conjugation channels for electron delivery powering CO_2 photoreduction. *Nat. Commun.* **2020**, *11*, 1149.
(64) Blochl, P. E. Projector augmented-wave method. *Phys. Rev. B: Condens. Matter Mater. Phys.* **1994**, *50*, 17953−17979.
(65) Perdew, J. P.; Burke, K.; Ernzerhof, M. Generalized gradient approximation made simple. *Phys. Rev. Lett.* **1996**, *77*, 3865−3868.

https://dx.doi.org/10.1021/jacs.0c09727
J. Am. Chem. Soc. 2020, 142, 20763−20771